Electronic Supplementary Material (ESI) for Journal of Materials Chemistry C.

SUPPORTING INFORMATION

TbCo and $Tb_{0.5}Dy_{0.5}Co$ layered cyanido-bridged frameworks for construction of colorimetric and ratiometric luminescent thermometers

Kunal Kumar,[a] Szymon Chorazy,[a,b] Koji Nakabayashi,[a] Hiroyasu Sato,[c] Barbara Sieklucka,[b] and Shin-ichi Ohkoshi*[a]*

[a]*Department of Chemistry, School of Science, The University of Tokyo, 7-3-1 Hongo, Bunkyo-ku, Tokyo, 113-0033, Japan.*

[b]*Faculty of Chemistry, Jagiellonian University, Gronostajowa 2, 30-387 Krakow, Poland.*

[c]*Rigaku Corporation, 3-9-12 Matsubaracho, Akishima-shi, Tokyo 196-8666, Japan.*

*Corresponding authors: ohkoshi@chem.s.u-tokyo.ac.jp; chorazy@chemia.uj.edu.pl

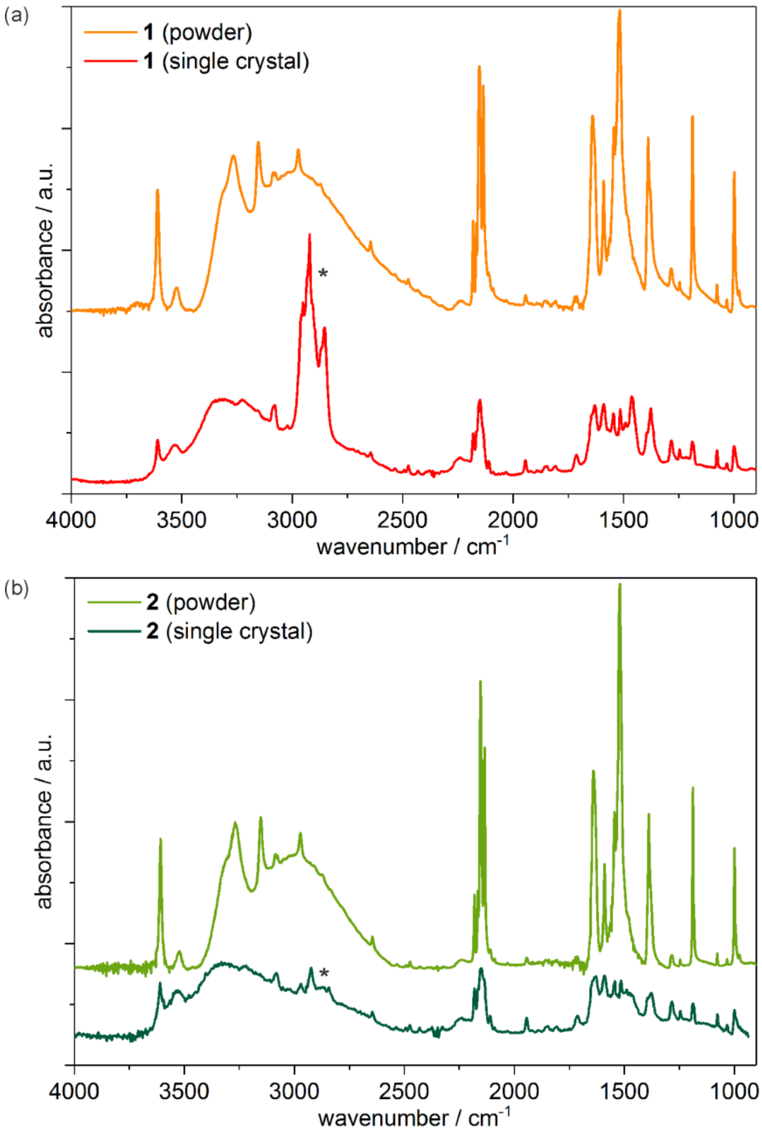

Figure S1. Comparison of the infrared absorption spectra of **1** and **2** measured for the powder polycrystalline samples mixed with potassium bromide and the selected single crystal mounted on calcium fluoride window by a small amount of paraffin oil. Note that the IR spectra for the single crystals are slightly affected by the applied paraffin oil, especially in the range marked by the asterisks.

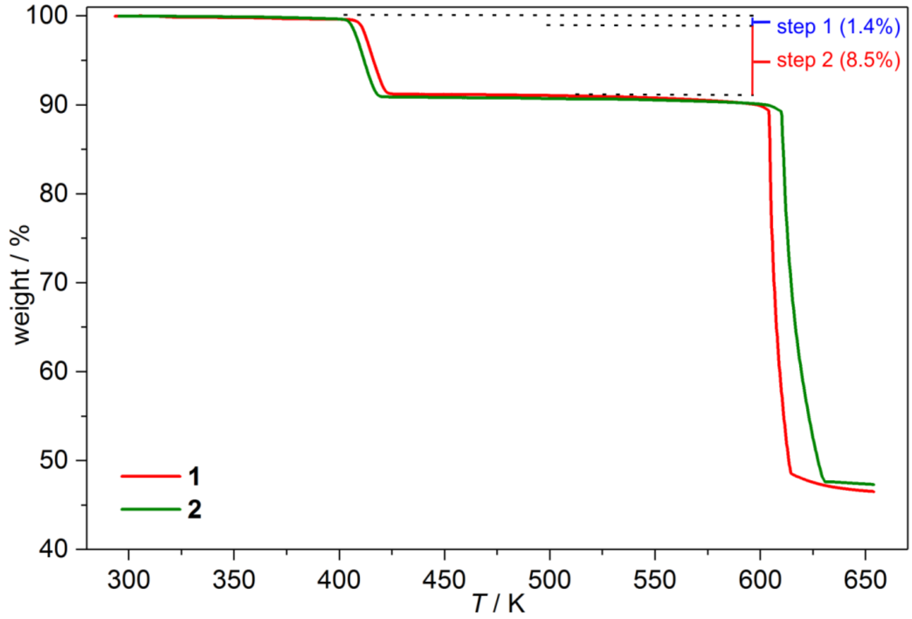

Figure S2. Thermogravimetric curves of **1** and **2** measured under an air atmosphere in the 293–653 K range with the indicated steps of the subsequent weight losses related to the removal of water molecules.

Comment to **Figure S2**:

The thermostability of **1** and **2** under the heating above room temperature was recorded using thermogravimetric techniques in the range of 293–653 K. Both materials show gradual small decrease of the mass between ca. 330 and 390 K from 100 % to 98.6 % (step 1). The related 1.4% weight loss can be attributed to the removal of weakly bonded non-coordinated water molecules in the amount of 0.5 molecule per {TbCo} and $\{Tb_{0.5}Dy_{0.5}Co\}$ units (calculated weight losses of 1.4%) for **1** and **2**, respectively. Further heating decreases the weight abruptly from 98.6% to 90.1% in the narrow range of 390–405 K (step 2). The related 8.6 % mass loss can be assigned to the removal of three coordinated water molecules per {LnCo} (Ln = Tb, Dy) unit (calculated weight loss of 8.6%). Thus, two-step weight loss can be ascribed to the dehydration of the samples, changing the composition from $\{[Ln(4\text{-}OHpy)_2(H_2O)_3][Co(CN)_6]\}.0.5H_2O$ to $\{[Ln(4\text{-}OHpy)_2][Co(CN)_6]\}$ (Ln = Tb, Dy). These results also confirm the room temperature compositions of **1** and **2**, found from CHN and metals elemental analyses (see Experimental). The dehydrated phases of $\{[Ln(4\text{-}OHpy)_2][Co(CN)_6]$ seem to be stable in the broad range of 405–620 K as indicated by the flat and long plateau. At higher temperatures, the mass of complexes decreases to 45%, which can be assigned to the typical loss of cyanides and expected decomposition of 4-OHpy, and/or reactivity with air present in the experimental conditions.

Table S1. Crystal data and structure refinement for **1**, compared with the analogous data for the previously reported isostructural $\{[\mathrm{Dy^{III}(4\text{-}OHpy)_2(H_2O)_3}][\mathrm{Co^{III}(CN)_6}]\}\cdot 0.5\mathrm{H_2O}$ compound.[S1]

compound		$\{[\mathrm{Tb(4\text{-}OHpy)_2(H_2O)_3}][\mathrm{Co(CN)_6}]\}\cdot 0.5\mathrm{H_2O}$ **1** (this work)	$\{[\mathrm{Dy(4\text{-}OHpy)_2(H_2O)_3}][\mathrm{Co(CN)_6}]\}\cdot 0.5\mathrm{H_2O}$ [ref. S1]
method		single-crystal XRD	single-crystal XRD
formula		$\mathrm{Tb_1Co_1C_{16}H_8N_8O_5}$	$\mathrm{Dy_1Co_1C_{16}H_{16}N_8O_5}$
formula weight		610.15 $\mathrm{g\cdot mol^{-1}}$	621.8 $\mathrm{g\cdot mol^{-1}}$
T [K]		90(2)	100(2)
λ [Å]		0.71073 (Mo Kα)	0.71073 (Mo Kα)
crystal system		monoclinic	monoclinic
space group		$P\,2_1/\mathrm{m}$ (no. 11)	$P\,2_1/\mathrm{m}$ (no. 11)
unit cell	***a*** [Å]	6.8969(7)	6.8970(5)
	b [Å]	15.6638(14)	15.6685(9)
	c [Å]	9.6068(10)	9.6096(6)
	β [deg]	102.059(10)	102.131(7)
V [Å^3]		1014.94(18)	1015.28(12)
Z		2	2
calcd. density		1.997	2.034
abs. coefficient		4.319	4.516
F(000)		584	602
crystal size [mm^3]		0.04×0.04×0.01	0.09 × 0.05 × 0.03
crystal type		colourless plate	colourless plate
Θ range [deg]		2.528–31.224	3.021–27.481
limiting indices		$-9 < h < 10$ $-21 < k < 21$ $-13 < l < 13$	$-8 < h < 8$ $-18 < k < 20$ $-11 < l < 12$
collected refls		18848	9618
unique refls		3174	2407
R_{int}		0.1016	0.0855
completeness		99.9 %	99.8 %
data/ restraints/parameters		3174/254/198	2407/41/185
GOF on F^2		1.524	1.208
final R indices		$R_1 = 0.1365$ [$I > 2\sigma(I)$] $wR_2 = 0.3592$ (all)	$R_1 = 0.0624$ [$I > 2\sigma(I)$] $wR_2 = 0.1119$ (all)
largest diff peak/hole		24.48/-4.90 $\mathrm{e\cdot A^{-3}}$	2.934/-2.729 $\mathrm{e\cdot A^{-3}}$

S1 S. Chorazy, J. Wang and S. Ohkoshi, *Chem. Commun.*, 2016, **52**, 10795.

Table S2. Detailed structure parameters of **1**.

Details of $[Co^{III}(CN)_6]^{3-}$ moiety		Details of $[Tb^{III}(4\text{-}OHpy)_2(H_2O)_3(CN)_3]$ moiety	
Parameter	Value	Parameter	Value
Co1–C1	1.899(14) Å	Tb1–O1	2.278(10) Å
Co1–C2	1.865(16) Å	Tb1–O2	2.467(13) Å
Co1–C3	1.920(15) Å	Tb1–O3	2.384(12) Å
Co1–C4	1.915(16) Å	Tb1–N2	2.527(18) Å
Co1–C5	1.948(19) Å	Tb1–N3	2.499(17)
C1–N1	1.14(2) Å	Tb1–N4	2.489(16)
C2–N2	1.11(2) Å	Tb1–N2–C2	171.0(16)°
C3–N3	1.14(2) Å	Tb1–N3–C3	154.5(16)°
C4–N4	1.12(2) Å	Tb1–N4–C4	161.1(15)°
C5–N5	1.16(3) Å	Tb1–O1–C8	149.4(9)°
Co1-C1-N1	176.8(12)°	N2–Tb1–N3	68.8(6)°
Co1-C2-N2	176.0(16)°	N3–Tb1–N4	156.9(6)°
Co1-C3-N3	172.9(16)°	N4–Tb1–N2	134.3(6)°
Co1-C4-N4	170.3(15)°	O1–Tb1–O1	75.3(5)°
Co1-C5-N5	173.5(19)°	O1–Tb1–O2	132.1(3)°
C1–Co1–C2	88.4(4)°	O2–Tb1–O3	72.3(3)°
C1–Co1–C3	91.3(4)°	O1–Tb1–N2	131.1(4)°
C1–Co1–C5	88.6(4)°	O1–Tb1–N3	80.0(4)°
C2–Co1–C4	176.0(6)°	O1–Tb1–N4	81.7(4)°
C2–Co1–C5	90.0(8)°	O2–Tb1–N2	65.9(5)°
C3–Co1–C4	95.7(7)°	O2–Tb1–N3	134.7(5)°
C3–Co1–C5	178.3(7)°	O2–Tb1–N4	68.4(5)°
C4–Co1–C5	86.0(8)°	O3–Tb1–N2	72.2(3)°
Co1–Tb1 (C2N2)	5.475 Å	O3–Tb1–N3	94.1(3)°
Co1–Tb1 (C3N3)	5.365 Å	O3–Tb1–N4	94.3(3)°
Co1–Tb1 (C4N4)	5.387 Å	(4-OHpy) – (4-OHpy) rings distance	5.709 Å

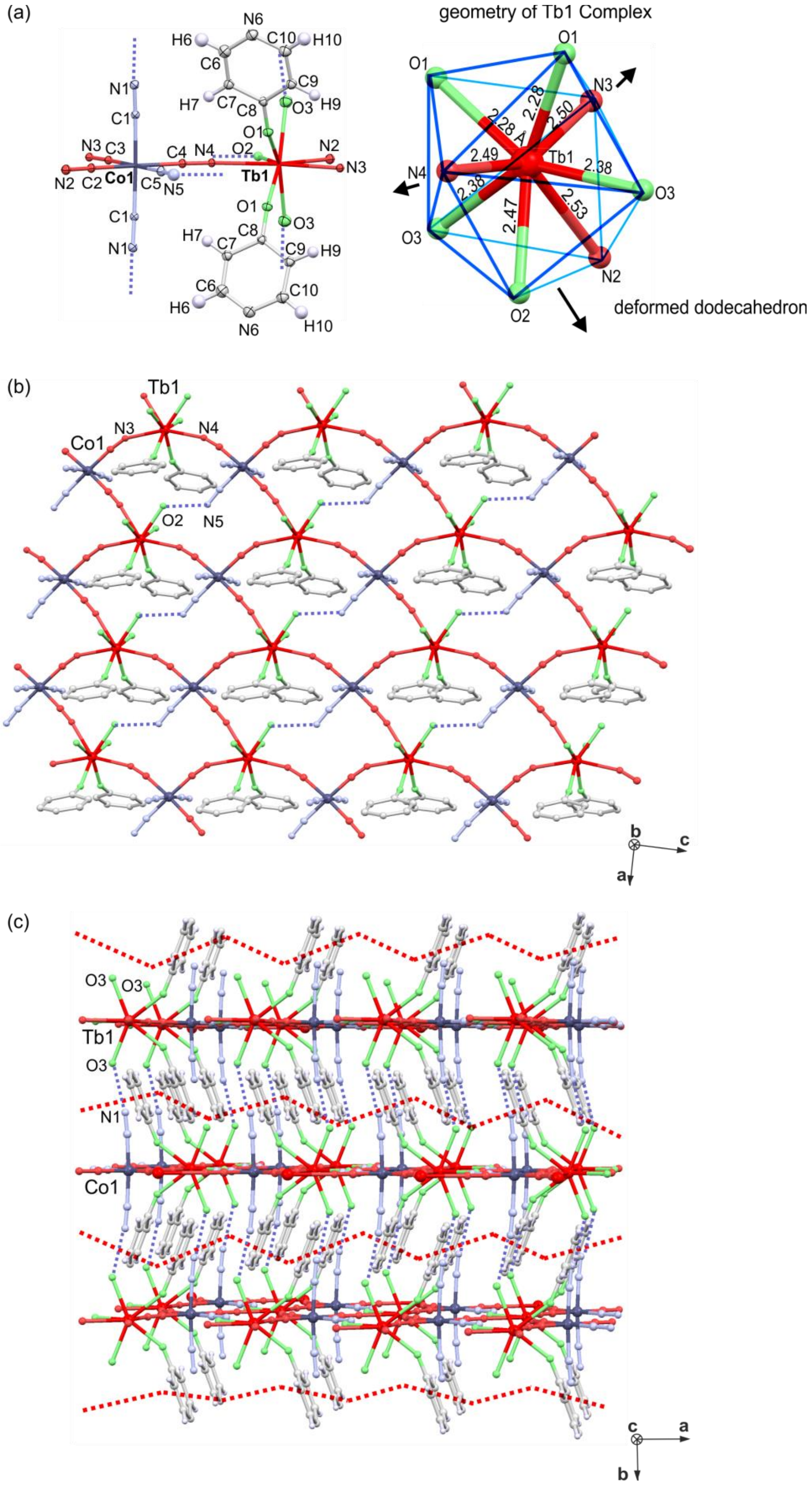

Figure S3. Detailed views of the crystal structure of **1**: (*a*) the representative molecular building unit with atoms labelling scheme along with structural insight into the geometry of the Tb1 complex, (*b*) the view of the cyanido-bridged layer with the indicated intralayer hydrogen bonds (black dotted lines), and (*c*) the supramolecular arrangement of the layers with the depicted interlayer hydrogen bonds (red dotted lines).

Table S3. Results of Continuous Shape Measure (CShM) analysis for [$\mathrm{Tb^{III}(NC)_3(4\text{-}OHpy)_2(H_2O)_3}$] complexes in the crystal structure of **1**

compound	CShM parameters*			geometry
	BTP-8	SAPR-8	DD-8	
1	2.749	3.216	0.495	DD-8

*CSM parameters:[S2]
CSM BTP-8 = the parameter related to the bicapped trigonal prism geometry (C_{2v} symmetry)
CSM SAPR-8 = the parameter related to the square antiprism (D_{4d} symmetry)
CSM DD-8 = the parameter related to the dodecahedron (D_{2d} symmetry)
CSM = 0 for the ideal geometry, and increases with the increasing distortion from the ideal polyhedron.

S2 (*a*) M. Llunell, D. Casanova, J. Cirera, J. Bofill, P. Alemany, S. Alvarez, M. Pinsky and D. Avnir, *SHAPE v. 2.1. Program for the Calculation of Continuous Shape Measures of Polygonal and Polyhedral Molecular Fragments*, University of Barcelona: Barcelona, Spain, 2013; (*b*) D. Casanova, J. Cirera, M. Llunell, P. Alemany, D. Avnir and S. Alvarez, *J. Am. Chem. Soc.*, 2004, **126**, 1755.

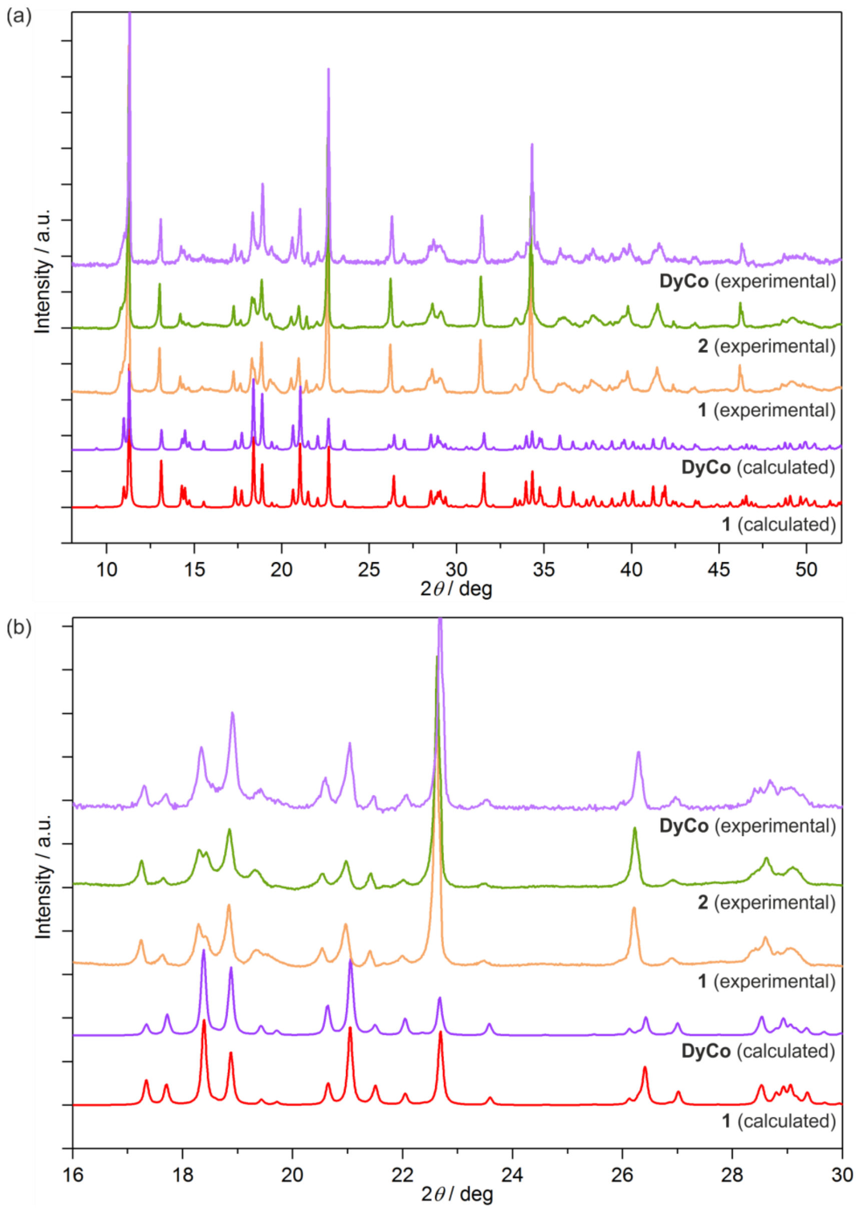

Figure S4. Experimental powder X-ray diffraction patterns of **1** and **2** compared with the experimental powder X-ray diffraction pattern of the analogous, previously reported $\{[Dy(4\text{-}OHpy)_2(H_2O)_3][Co(CN)_6]\}\cdot 0.5H_2O$ (**DyCo**) compound,[S1] and with the related patterns of **1** and **DyCo** calculated from the respective structural models of the single crystal X-ray diffractions analyses. In (*a*) the broad 5–50° range of 2*Θ* angle was presented when the (*b*) part shows the enlargement of the representative 2*Θ* range of 16–30°. The consequent shift of the diffraction peaks between calculated and experimental patterns is due to the temperature effect as the single-crystal X-ray diffraction measurement was performed at 90(2) K (**1**) or 100(2) K (**DyCo**), while the powder X-ray diffraction experiments at room temperature. The **DyCo** compound was prepared according to the published procedure.[S1]

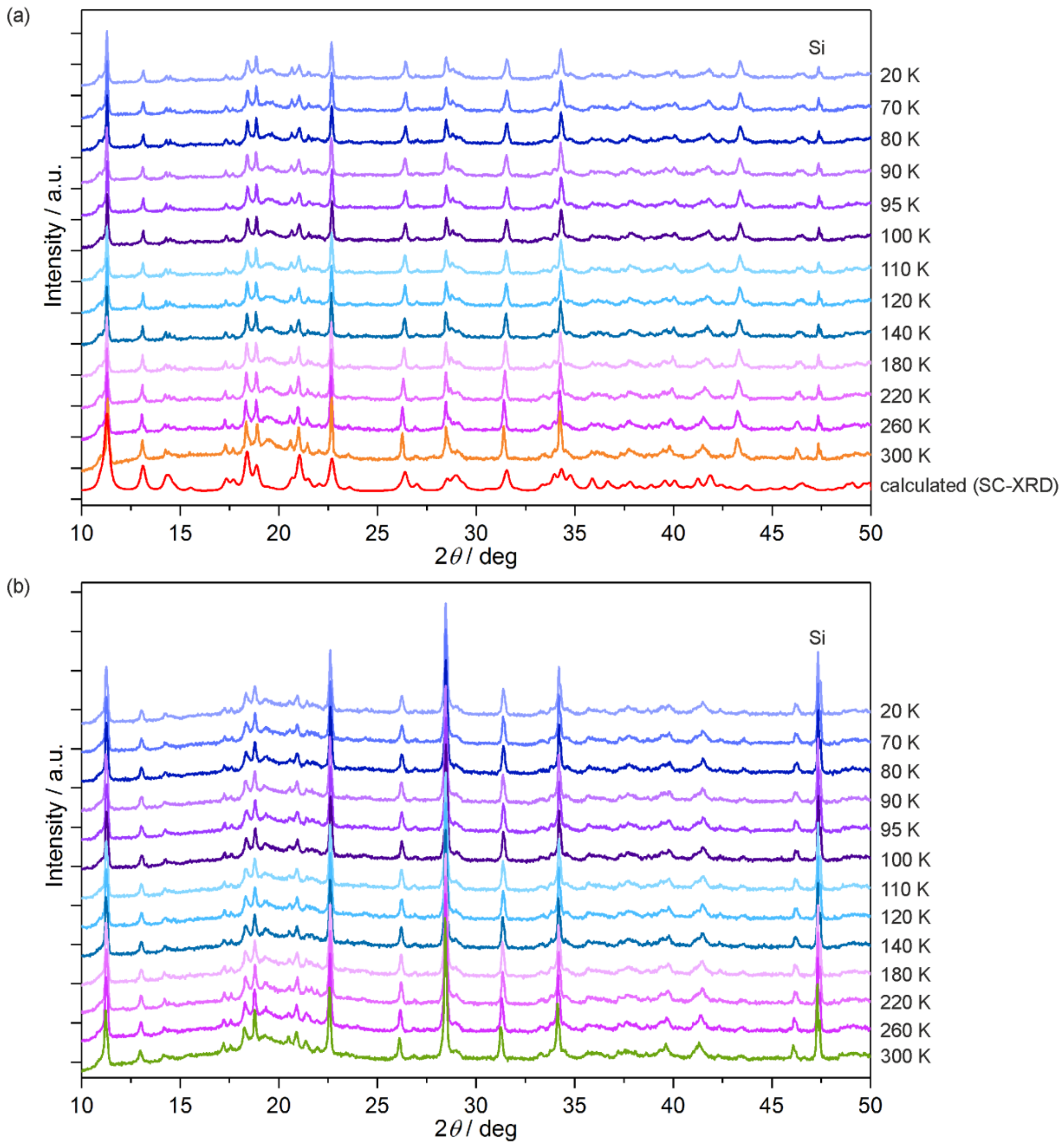

Figure S5. Temperature variable powder X-ray diffraction patterns of **1** (*a*) and **2** (*b*) presented at the indicated temperatures from the 20–300 K range. For (*a*), the comparison with the calculated pattern based on the single-crystal X-ray diffraction (SC-XRD) model obtained from the measurement at 90(2) K was additionally shown. The peak originated from Si used a temperature reference material was indicated.

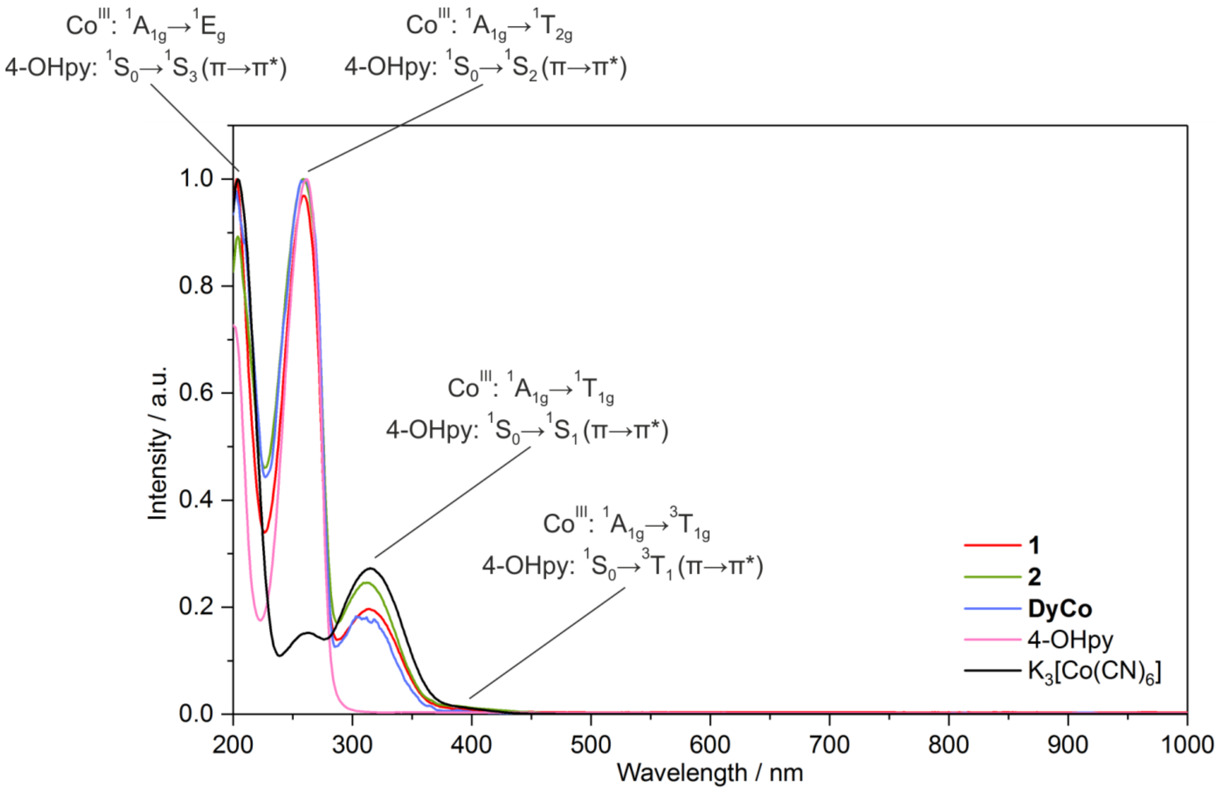

Figure S6. Room temperature solid-state UV-Vis-NIR absorption (Kubelka-Munk function) spectra of **1** and **2** compared with the relevant spectra of 4-OHpy and $K_3[Co(CN)_6]$, as well as with the spectrum of the previously reported $\{[Dy(4\text{-}OHpy)_2(H_2O)_3][Co(CN)_6]\}\cdot 0.5H_2O$ (**DyCo**) compound.[S1] The intensities of the spectra were scaled in relation to the maxima at ca. 200 nm for the a given intensity of 1.0. The assignment of the main contributions to the absorption bands was indicated on the graphs.

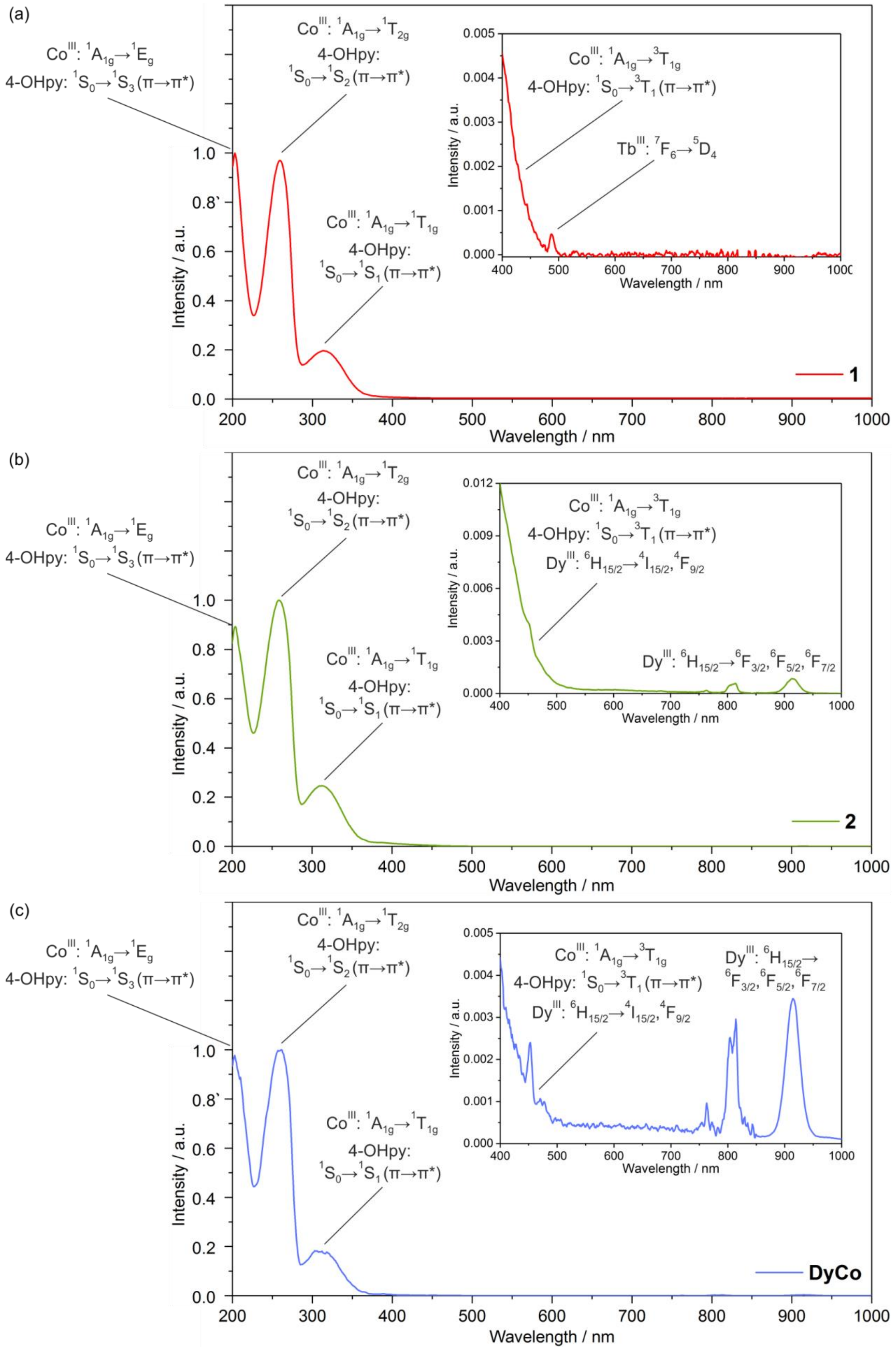

Figure S7. Detailed insight into the room temperature solid-state UV-Vis-NIR absorption (Kubelka-Munk function) spectra of **1** (*a*), **2** (*b*), and previously reported $\{[Dy(4\text{-OHpy})_2(H_2O)_3][Co(CN)_6]\}\cdot 0.5H_2O$ (**DyCo**) compound (*c*),[S1] with the enlargement of the Vis-NIR region showing the lanthanide(III)-centered electronic transitions. The assignment of the main absorption bands was indicated on the graphs.

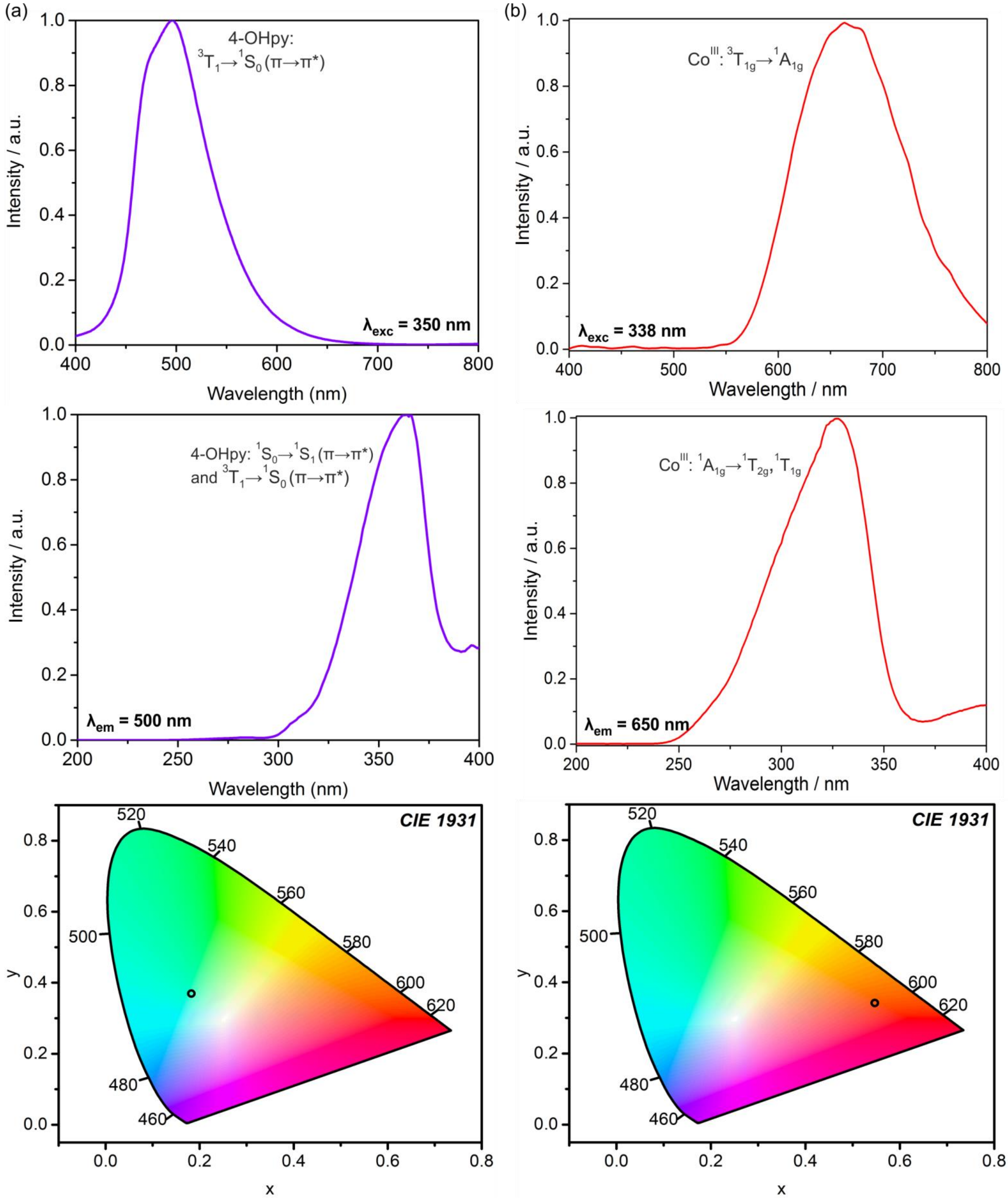

Figure S8. Low temperature (*T* = 77 K) solid state UV-Vis-NIR emission and excitation spectra of 4-hydroxy-pyridine (*a*) and potassium hexacyanidocobaltate(III) (*b*) together with the related CIE 1931 chromaticity diagrams. The assignment of the main contributions to the excitation and emission bands was indicated on the graphs.

Table S4. Summary of *xy* parameters of the CIE 1931 chromaticity scale for the emission colours of **1** and **2** detected at room temperature (T = 298 K) and low temperature (T = 77 K) under various indicated wavelengths of excitation light.

compound	T / K	λ_{exc} / nm	x	y
1 (Figure 3)	298	270	0.528	0.452
		300	0.552	0.435
		325	0.551	0.428
		335	0.528	0.403
		340	0.491	0.382
		345	0.408	0.356
		350	0.322	0.348
		352	0.275	0.338
		355	0.197	0.333
		362	0.129	0.339
	77	270	0.303	0.576
		300	0.328	0.553
		336	0.307	0.582
		377	0.284	0.476
2 (Figure 4)	298	270	0.361	0.473
		275	0.392	0.425
		285	0.438	0.394
		300	0.506	0.385
		325	0.402	0.356
		332	0.317	0.317
		335	0.253	0.287
		338	0.202	0.278
		349	0.157	0.355
		362	0.124	0.402
	77	270	0.301	0.598
		325	0.320	0.595
		349	0.314	0.556
		362	0.314	0.559

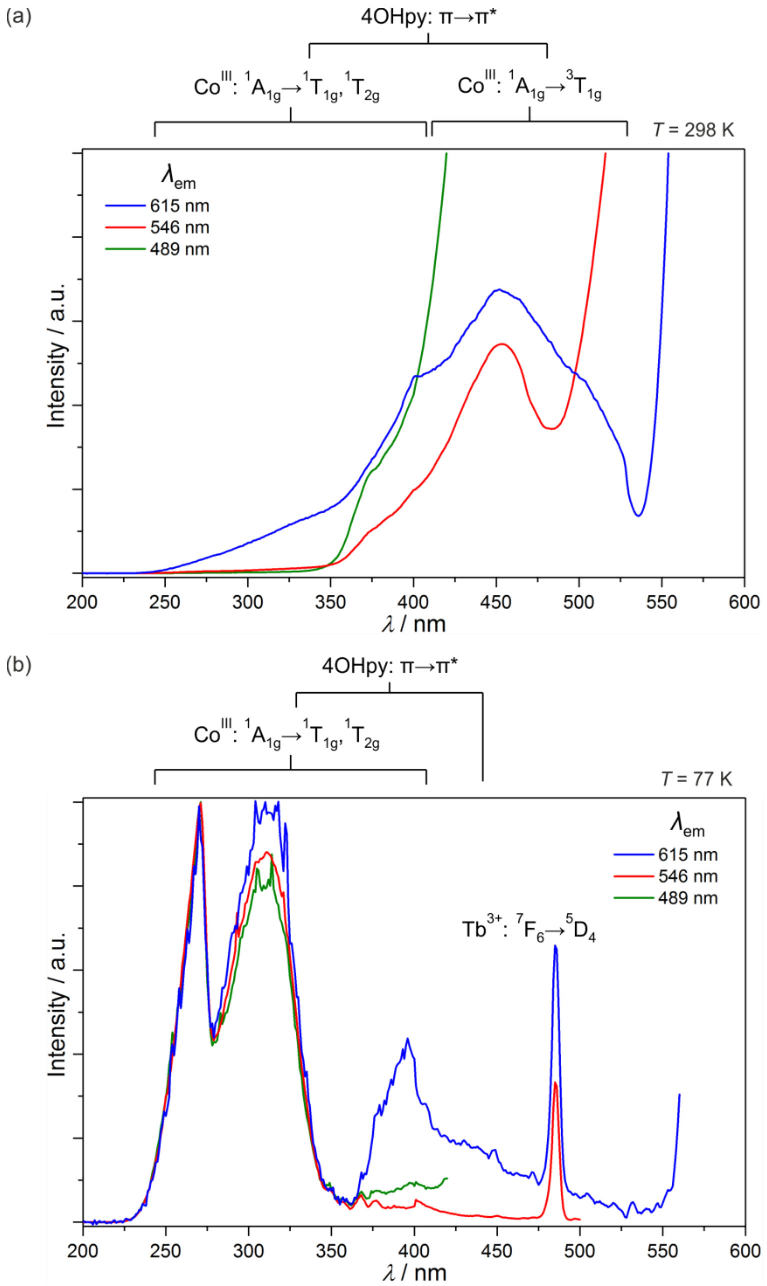

Figure S9. Room temperature (*a*, $T = 298$ K) and low temperature (*b*, $T = 77$ k) solid-state excitation spectra of **1** in the broad UV-Vis range for the indicated emission wavelengths. The assignments of the main excitation peaks were indicated on the graphs.

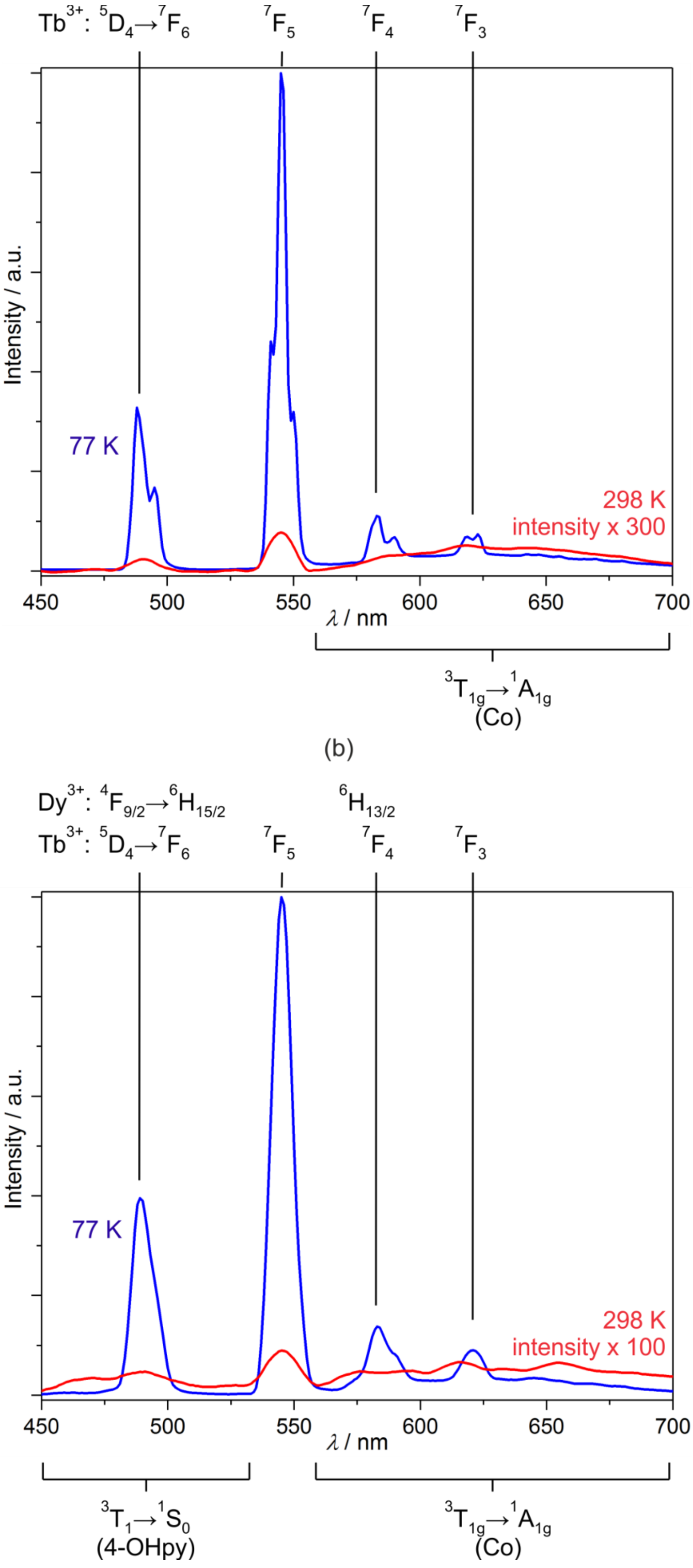

Figure S10. Room temperature (T = 298 K) and low temperature (T = 77 K) solid state UV-Vis-NIR emission spectra of **1** (*a*) and **2** (*b*) by the 325 nm light. The assignment of the main excitation and emission bands was indicated on the graphs. For clarity, the intensities of the room temperature spectra were multiplied by the indicated values.

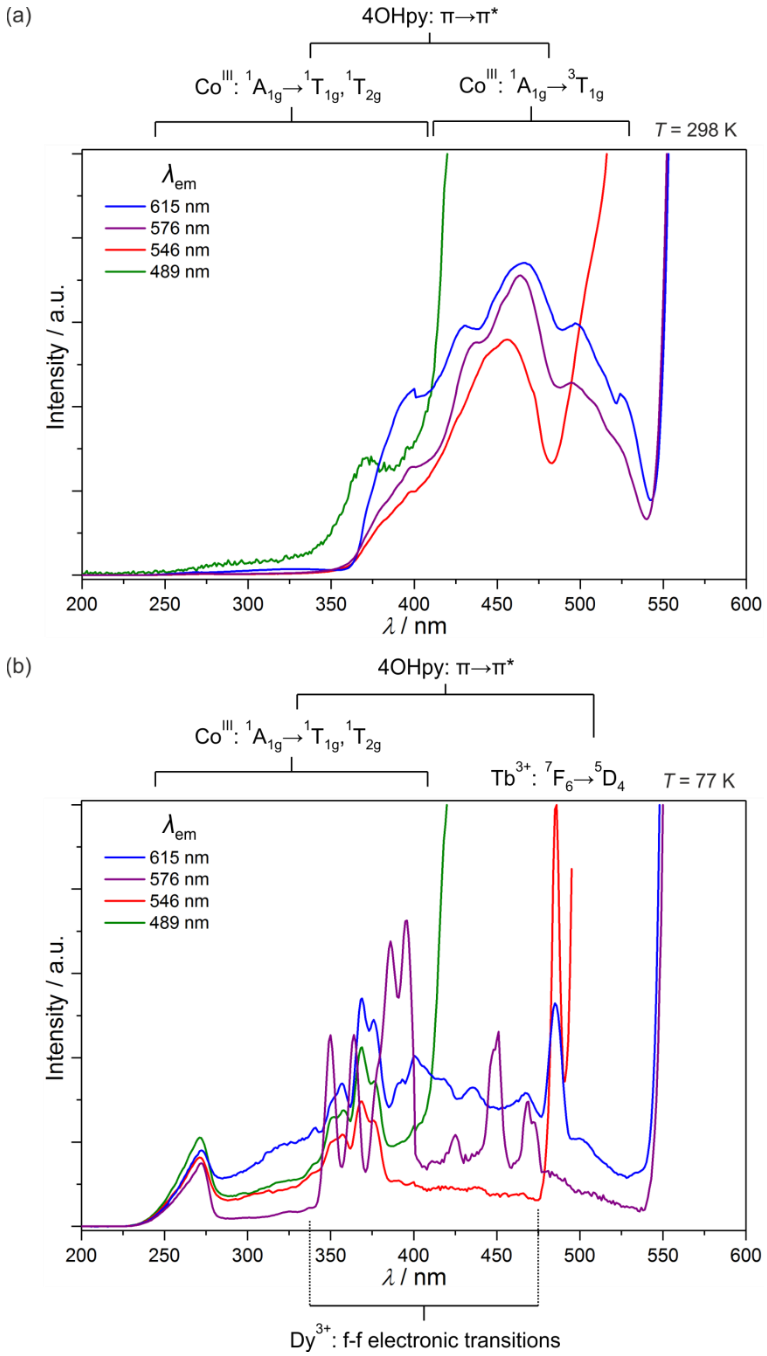

Figure S11. Room temperature (*a*, $T = 298$ K) and low temperature (*b*, $T = 77$ k) solid-state excitation spectra of **2** in the broad UV-Vis range for the indicated emission wavelengths. The assignments of the main excitation peaks were indicated on the graphs.

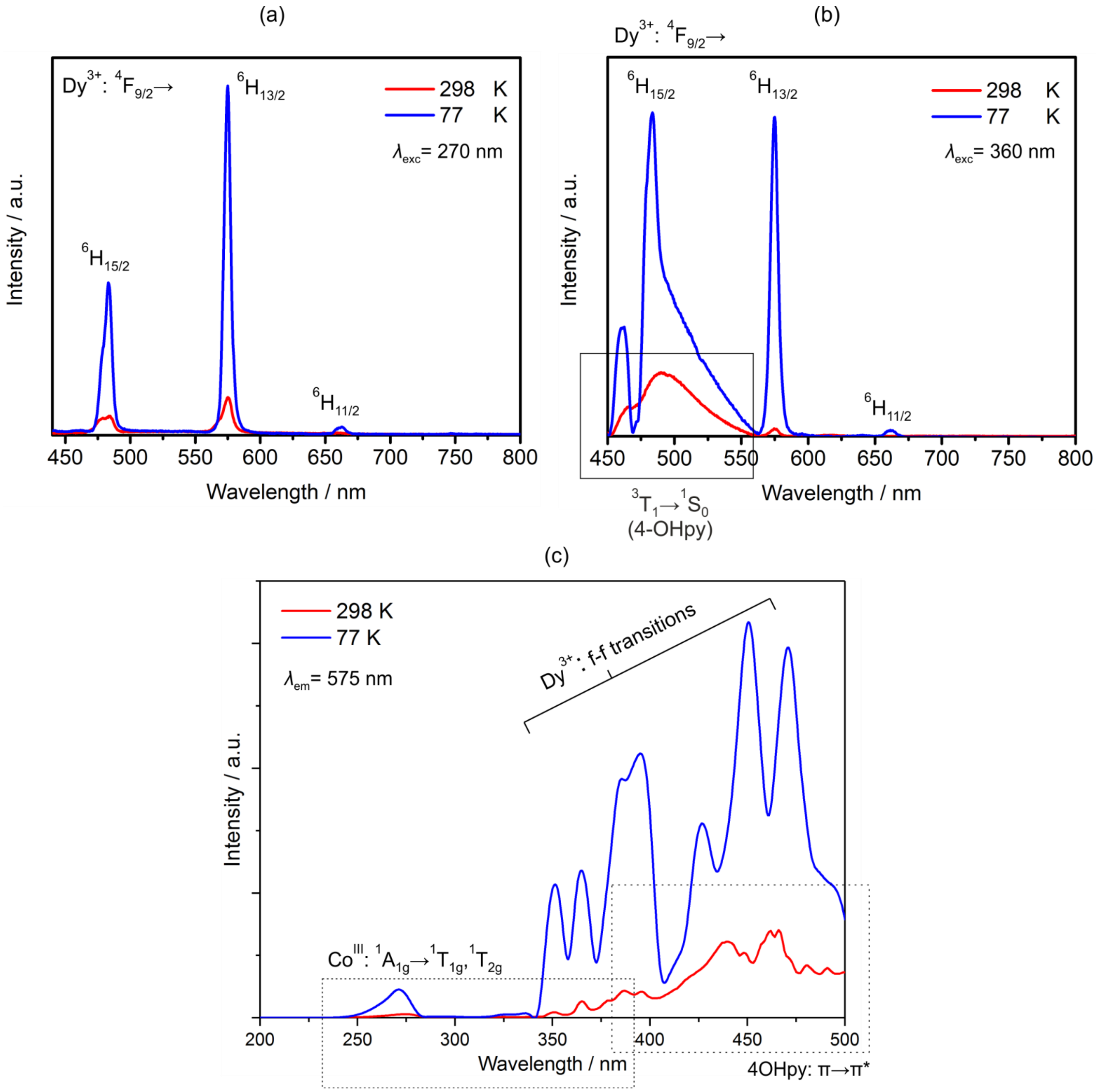

Figure S12. Room temperature (T = 298 K) and low temperature (T = 77 K) solid state UV-Vis-NIR emission spectra of previously reported $\{[Dy(4\text{-}OHpy)_2(H_2O)_3][Co(CN)_6]\}\cdot 0.5H_2O$ (**DyCo**) compound under the excitation by the 270 nm (*a*) and 360 nm (*b*) light, and the related excitation spectra for the monitored emission of 575 nm. The assignment of the main excitation and emission bands was indicated on the graphs.

Table S5. Summary of *xy* parameters of the CIE 1931 chromaticity scale for the emission colours of **1** and **2** under the excitation by the 325 nm light at various indicated temperatures.

compound	T / K	x	y
1 (Figure 6)	300	0.523	0.432
	280	0.516	0.443
	260	0.509	0.462
	240	0.480	0.483
	220	0.444	0.501
	200	0.407	0.530
	180	0.371	0.559
	160	0.344	0.575
	140	0.321	0.581
	120	0.316	0.587
	100	0.321	0.584
	90	0.326	0.580
	80	0.333	0.574
	70	0.342	0.568
2 (Figure 7)	300	0.488	0.430
	280	0.504	0.450
	260	0.457	0.462
	240	0.457	0.494
	220	0.418	0.515
	200	0.388	0.542
	180	0.358	0.562
	160	0.323	0.576
	140	0.321	0.577
	120	0.318	0.577
	110	0.314	0.583
	100	0.316	0.579
	90	0.320	0.576
	80	0.324	0.574
	70	0.325	0.574

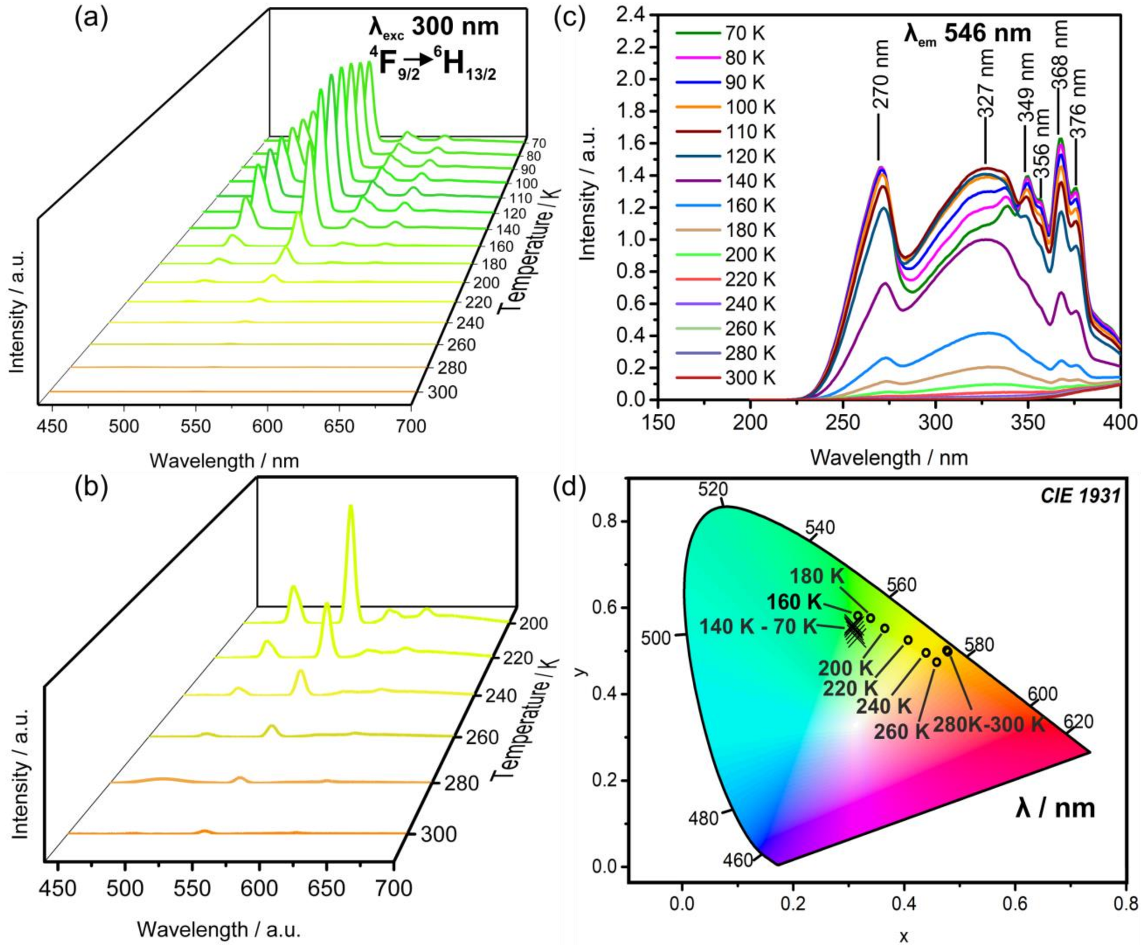

Figure S13. Solid state visible light emission spectra of **2** recorded at various indicated temperatures from the 300–70 K range upon excitation by the 300 nm light (*a*), together with enlargement of the high temperature region (*b*), the related excitation spectra for the monitored emission of 546 nm (*c*), and the respective emission colours presented on the CIE 1931 chromaticity diagram (*d*).

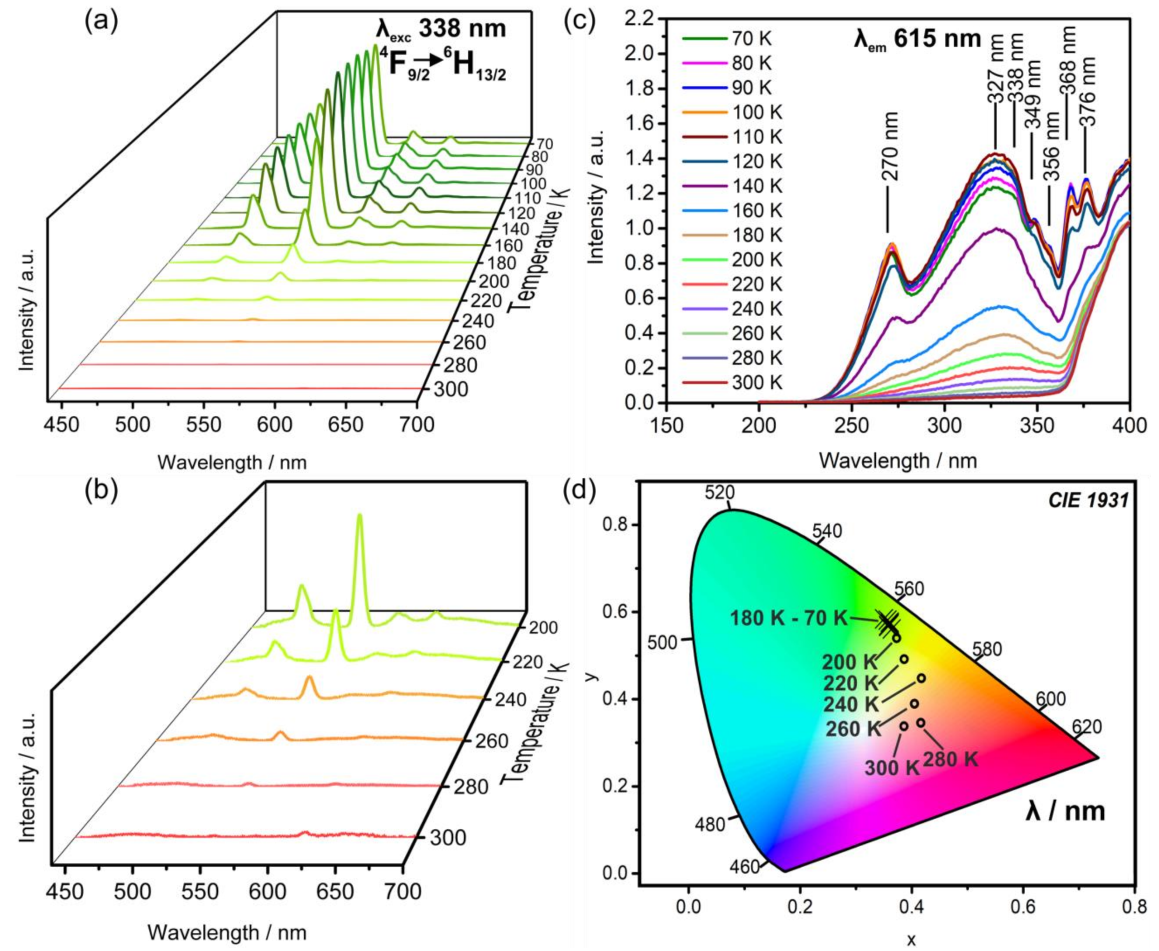

Figure S14. Solid state visible light emission spectra of **2** recorded at various indicated temperatures from the 300–70 K range upon excitation by the 338 nm light (*a*), together with enlargement of the high temperature region (*b*), the related excitation spectra for the monitored emission of 615 nm (*c*), and the respective emission colours presented on the CIE 1931 chromaticity diagram (*d*).

Table S6. Summary of *xy* parameters of the CIE 1931 chromaticity scale for the emission colours of **2** under two selected excitation wavelengths suitable for colorimetric temperature sensing.

excitation wavelength	T / K	x	y
300 nm (Figure S13)	300	0.479	0.498
	280	0.477	0.501
	260	0.459	0.474
	240	0.439	0.496
	220	0.407	0.525
	200	0.365	0.552
	180	0.339	0.576
	160	0.316	0.581
	140	0.311	0.558
	120	0.309	0.563
	110	0.308	0.558
	100	0.309	0.554
	90	0.311	0.547
	80	0.313	0.540
	70	0.315	0.530
338 nm (Figure S14)	300	0.386	0.338
	280	0.416	0.389
	260	0.405	0.448
	240	0.386	0.492
	220	0.373	0.540
	200	0.526	0.440
	180	0.361	0.577
	160	0.361	0.573
	140	0.360	0.571
	120	0.358	0.568
	110	0.357	0.569
	100	0.358	0.567
	90	0.364	0.561
	80	0.357	0.581
	70	0.350	0.584

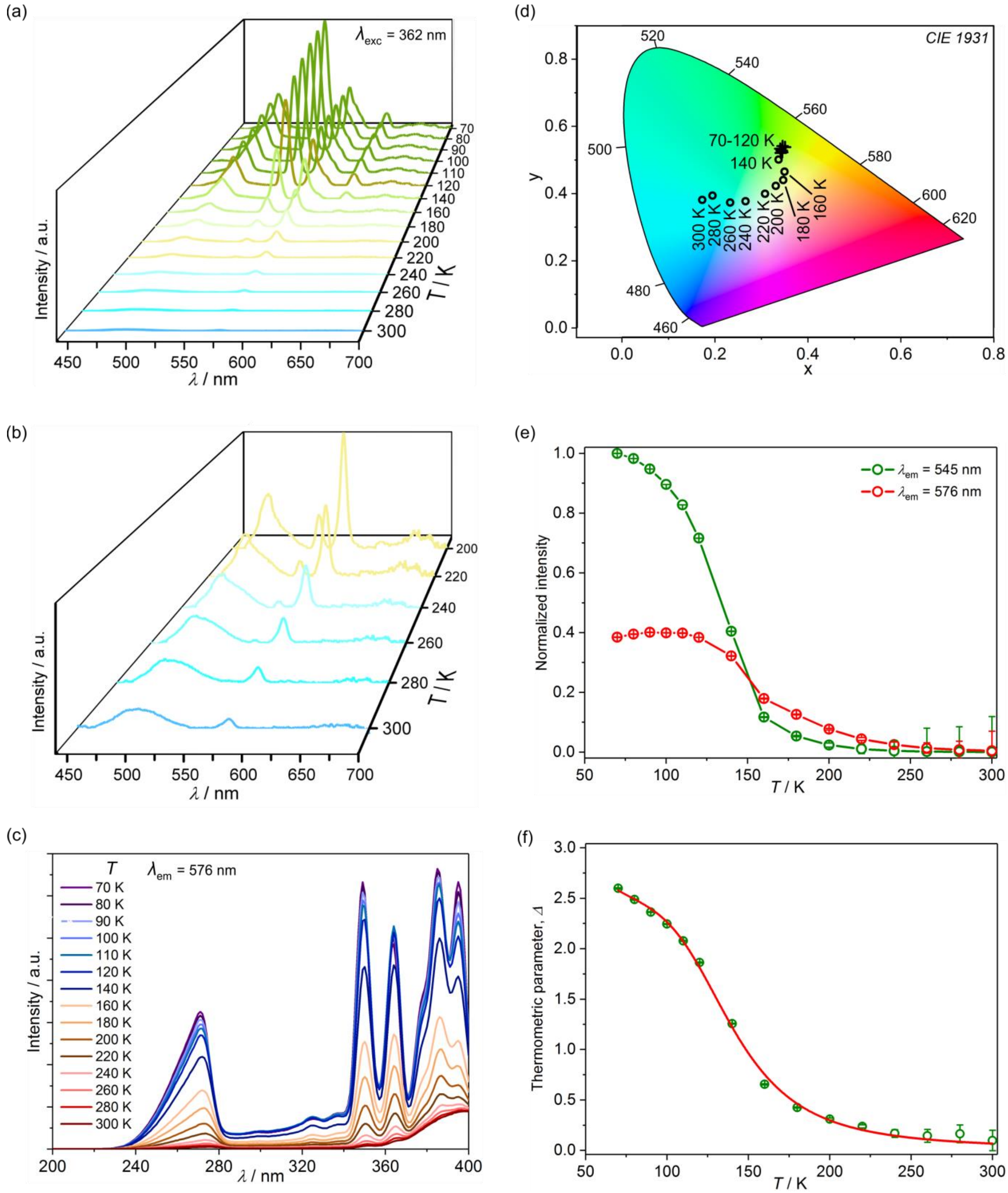

Figure S15. Solid state visible light emission spectra of **2** recorded at various indicated temperatures from the 300–70 K range upon excitation by the 362 nm light (*a*), together with enlargement of the high temperature region (*b*), the related excitation spectra for the monitored emission of 576 nm (*c*), and the respective emission colours presented on the CIE 1931 chromaticity diagram (*d*). In addition, the part (*e*) shows the temperature dependence of the normalized intensities of the 545 and 576 nm peaks related to the $^5D_4 \rightarrow {}^7F_5$ Tb^{III}-based (I_{Tb}) and $^4F_{9/2} \rightarrow {}^6H_{13/2}$ Dy^{III}-based (I_{Dy}) transitions, respectively, while the part (*f*) presents the temperature dependence of the thermometric parameter, Δ, defined as the emission intensities ratio, I_{Tb}/I_{Dy}, together with the calibration curve (solid line) obtained by the best fit ($R^2 = 0.997$) following the classical Mott-Seitz model involving two non-radiative recombination channels (see text of the manuscript for details).

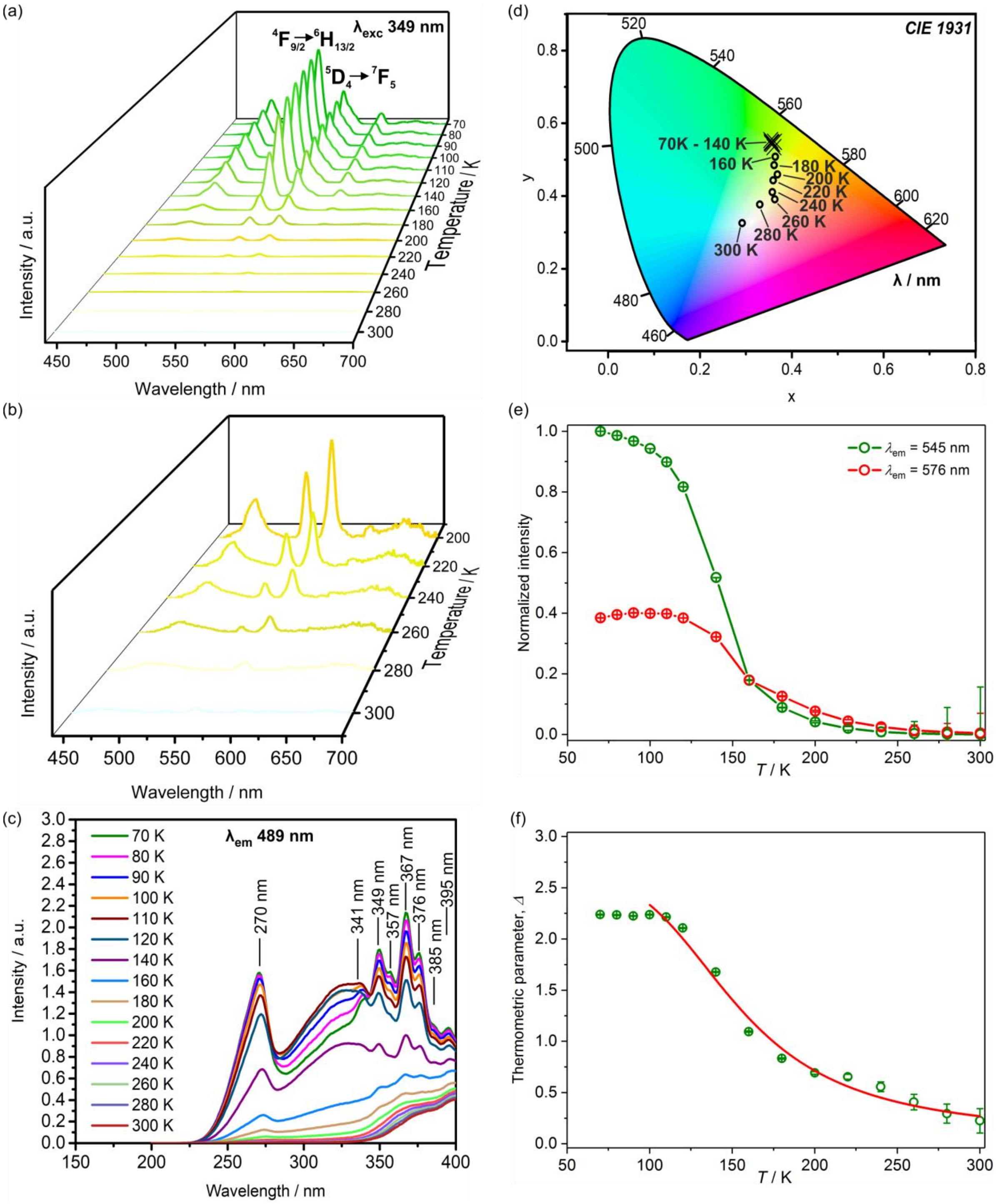

Figure S16. Solid state visible light emission spectra of **2** recorded at various indicated temperatures from the 300–70 K range upon excitation by the 349 nm light (*a*), together with enlargement of the high temperature region (*b*), the related excitation spectra for the monitored emission of 576 nm (*c*), and the respective emission colours presented on the CIE 1931 chromaticity diagram (*d*). In addition, the part (*e*) shows the temperature dependence of the normalized intensities of the 545 and 576 nm peaks related to the $^5D_4 \rightarrow {}^7F_5$ Tb^{III}-based (I_{Tb}) and $^4F_{9/2} \rightarrow {}^6H_{13/2}$ Dy^{III}-based (I_{Dy}) transitions, respectively, while the part (*f*) presents the temperature dependence of the thermometric parameter, Δ, defined as the emission intensities ratio, I_{Tb}/I_{Dy}, together with the calibration curve (solid line) obtained by the best fit (R^2 = 0.986) following the classical Mott-Seitz model involving two non-radiative recombination channels (see text of the manuscript for details).

Table S7. Summary of *xy* parameters of the CIE 1931 chromaticity scale for the emission colours of **2** under two selected excitation wavelengths suitable for colorimetric and ratiometric temperature sensing.

excitation wavelength	T / K	x	y
270 nm (Figure 8)	300	0.361	0.473
	280	0.356	0.460
	260	0.355	0.471
	240	0.342	0.461
	220	0.366	0.470
	200	0.344	0.483
	180	0.325	0.498
	160	0.311	0.512
	140	0.307	0.537
	120	0.300	0.547
	110	0.298	0.545
	100	0.298	0.543
	90	0.296	0.541
	80	0.302	0.550
349 nm (Figure S16)	300	0.292	0.325
	280	0.330	0.378
	260	0.363	0.391
	240	0.358	0.411
	220	0.359	0.443
	200	0.369	0.460
	180	0.362	0.485
	160	0.364	0.508
	140	0.355	0.548
	120	0.357	0.547
	110	0.362	0.549
	100	0.356	0.545
	90	0.354	0.554
	80	0.361	0.534
	70	0.358	0.543
362 nm (Figure S15)	300	0.173	0.381
	280	0.195	0.394
	260	0.233	0.373
	240	0.266	0.377
	220	0.308	0.399
	200	0.331	0.423
	180	0.347	0.440
	160	0.350	0.465
	140	0.337	0.501
	120	0.343	0.524
	110	0.346	0.526
	100	0.352	0.541
	90	0.345	0.531
	80	0.342	0.536
	70	0.347	0.544

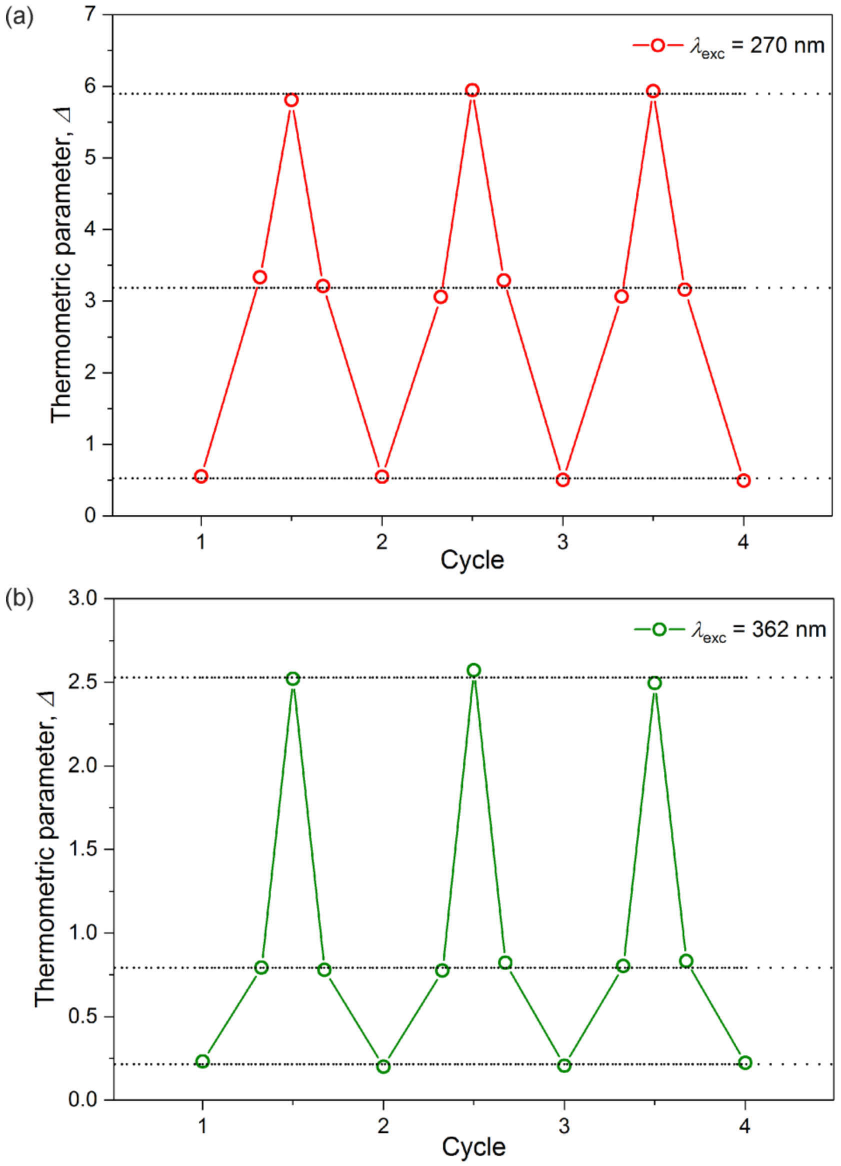

Figure S17. Trend of thermometric parameter, Δ for **2** under the excitation by 270 nm (*a*) and 362 nm (*b*) light during temperature cycling between 300 and 70 K revealing the repeatability > 97 % for both excitation wavelengths.